Quaternary Research (2025), **123**, 1–15
doi:10.1017/qua.2024.38

Research Article

A high-resolution record of Late Holocene drought in the eastern Sierra Nevada (California, USA) from June Lake carbonate geochemistry

Eva C. Lyon[a,b], Andrea M. Erhardt[a], Laura C. Streib[a,c], Susan R.H. Zimmerman[d] and Michael M. McGlue[a]

[a]Department of Earth and Environmental Sciences, University of Kentucky, Lexington, Kentucky 40506, USA; [b]Department of Earth Sciences, The College of Wooster, Wooster, Ohio 44691, USA; [c]Syracuse University, Department of Earth and Environmental Sciences, Syracuse, New York 13244, USA and [d]Center for Accelerator Mass Spectrometry, Lawrence Livermore National Laboratory, Livermore, California 94550, USA

Abstract

As historic drought conditions become more common in western North America, Late Quaternary hydroclimate records become vital for putting present anthropogenic conditions into a longer-term context. Here, we establish a high-resolution record of drought for the eastern Sierra Nevada (California) using lacustrine carbonates from well-dated sediment cores. We used oxygen and carbon stable-isotope ratios, combined with high-resolution scanning X-ray fluorescence counts of calcium (Ca) and titanium (Ti), to reconstruct the drought record over the last 4600 years in June Lake. We found elevated $\delta^{18}O$ and $\delta^{13}C$ carbonate isotope values coinciding with peaks in both total inorganic carbon and Ca/Ti, suggesting enhanced carbonate precipitation in response to evaporative concentration of lake water. At least six intervals of prolonged (centennial-scale) carbonate deposition were identified, including three pulses during the Late Holocene Dry Period (LHDP; ~3500–2000 cal yr BP), the Medieval Climate Anomaly (~1200–800 cal yr BP), and the Current Warm Period, which began around 100 cal yr BP. This record highlights the complexities of the LHDP, an interval that was more variable at June Lake than has been previously described in regional records.

Keywords: Stable isotopes, paleolimnology, Late Holocene Dry Period, lake sediment, paleoclimatology, paleohydrology, glacial lake, Quaternary, sediment core, climate change

Introduction

The western United States has recently experienced the worst drought in the last 1200 years (Williams et al., 2022). Highly resolved paleorecords of drought from the western United States are vital for contextualizing contemporary hydroclimate and providing an archive of the potential limnological changes that accompany them. High-resolution paleoclimate proxy records are also potentially useful in assessing climate models in order to better plan for future environmental variability (e.g., Braconnot et al., 2012; Kaufman et al., 2020). This is particularly true in California, a state with a population of ~40 million people and an agricultural sector that earned ~$51.1 billion in 2021 (https://cdfa.ca.gov/statistics, accessed June 19, 2023). Much of this population is served by water sources from the Sierra Nevada snowpack (e.g., Huang et al., 2018; Sun et al., 2019), which is at risk from hazards like extreme droughts, floods, and wildfires (e.g., Diffenbaugh et al., 2015; Ullrich et al., 2018; Goss et al., 2020). With these issues in mind, we seek to establish a robust record of Late Holocene hydroclimate variability for the eastern Sierra Nevada using carbonates from June Lake (Fig. 1).

A key objective of this study is to resolve the paleohydrological conditions associated with the Late Holocene Dry Period (LHDP) and Medieval Climate Anomaly (MCA) in the eastern Sierra Nevada. Evidence of the LHDP has been observed in paleoclimatic and paleoecological archives across the Great Basin (e.g., Mensing et al., 2013, 2023; Thiessen et al., 2019), including Mono Lake (Fig. 1; Zimmerman et al., 2021). Those sediment proxy records are relatively low resolution, and define the LHDP as a multicentury drought. Because the sediments of June Lake have relatively high accumulation rates, their proxy data sets, including carbonate stable isotopes ($\delta^{18}O_{carb}$ and $\delta^{13}C_{carb}$, which we hereafter refer to as carbonate isotopes) and X-ray fluorescence (XRF) geochemistry, have the potential to show discrete decadal to centennial-scale droughts within this broader LHDP window, as well as other parts of the Late Holocene. Thus, we seek to apply these data to determine whether the LHDP was a single multicentury dry period or multiple shorter droughts.

Study area

June Lake (Mono County California, 37°47′17″N, 119°4′23″W) occupies a glacial scour basin at the foot of the eastern Sierra

Corresponding author: Eva C. Lyon; Email: evlyon@wooster.edu

Cite this article: Lyon EC, Erhardt AM, Streib LC, Zimmerman SRH, McGlue MM (2025). A high-resolution record of Late Holocene drought in the eastern Sierra Nevada (California, USA) from June Lake carbonate geochemistry. *Quaternary Research* **123**, 1–15. https://doi.org/10.1017/qua.2024.38

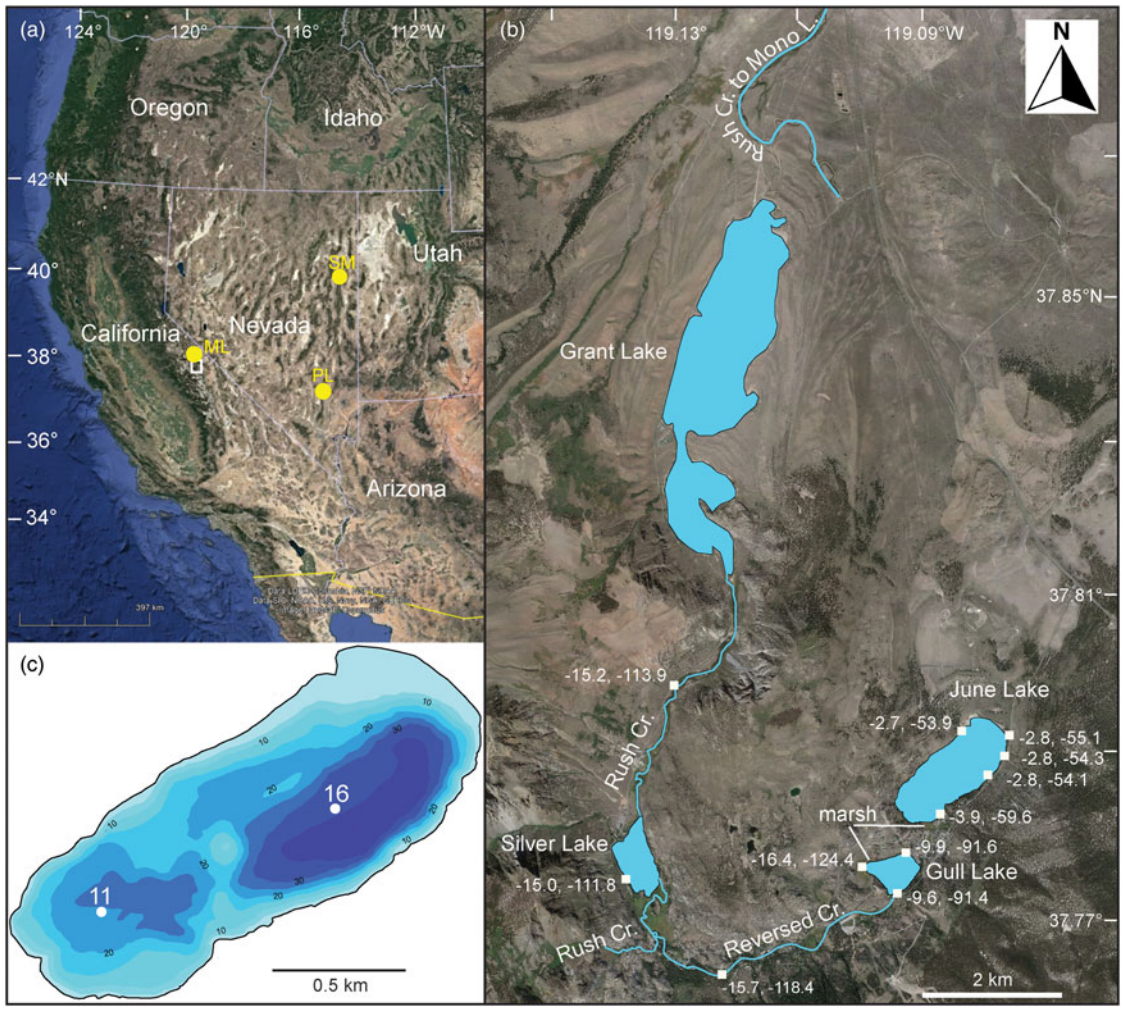

Figure 1. (A) Regional map showing location of study area (white box) and locations of other records discussed in the text (yellow circles): ML, Mono Lake; SM, Stonehouse Meadow; PL, Pahranagat Lake. (B) Lakes and streams of the study area, which are found along CA State Route 158 (the June Lake Loop). Water isotope values for locations indicated by white squares (oxygen, deuterium). (C) June Lake bathymetric map (after Lyon et al., 2019). White circles indicate locations of the cores discussed in this study. Base images for (A) and (B) are from Google Earth®.

Nevada at a surface elevation of 2324 meters above sea level. It is an oligotrophic to mesotrophic lake that is seasonally stratified in warmer months (Lyon et al., 2019). Seismic stratigraphic analysis revealed that June Lake has two deepwater depocenters separated by a bedrock shoal; the deeper of the two has a maximum depth of 42 m (Fig. 1; Lyon et al., 2019). Sediments accumulating in these depocenters are organic-matter-rich laminated oozes with variable carbonate concentrations (Lyon et al., 2019).

The paleoproduction and environmental history of June Lake were first described using low-resolution organic matter geochemical records (Lyon et al., 2020). That study defined four chronological zones based on paleoproduction and inferred hydroclimate variation within a 4600-year-long sediment sequence collected from the southwestern depocenter. Using a core from the northeastern depocenter, Streib et al. (2021) established a diatom paleoecological record of lake stratification and nutrient cycling over the last two millennia. Streib et al. (2021) found that the algal community has become both more diverse and less productive over the last ~150 years, owing to the influence of climate warming on water-column stratification.

June Lake is fed by seasonal snowmelt runoff and groundwater discharge from subaqueous springs (Fig. 1). At present, there are no surface outlets, though a low, marshy terrain at the southwestern end of the basin is only a few meters higher than neighboring Gull Lake (Lopera-Congote et al., 2024) (Fig. 1). Lyon et al. (2020) and Streib et al. (2021) proposed that during some high stands, June Lake likely spilled over and connected the two basins during wetter time periods, resulting in an open lake system that flowed out through Reversed Creek. Reversed Creek, to our knowledge the only westward-directed stream east of the Sierran crest, joins Rush Creek prior to entering Silver Lake, which is open at its downstream end (Fig. 1). Rush Creek flows into Grant Lake reservoir before flowing out over a dam and into endorheic Mono Lake from the south. This chain of waterbodies parallels California Highway 158 (i.e., the June Lake Loop) (Fig. 1).

Regional climate

The study region has a Mediterranean climate; summers are typically dry and warm (highs in the mid-20s °C), and most of the ~40 cm of total annual precipitation falls as snow (~180 cm, or about 30 cm calculated snow water equivalent) in the winter months, which have average low temperatures around −11°C (National Oceanic and Atmospheric Administration,

https://doi.org/10.1017/qua.2024.38 Published online by Cambridge University Press

https://www.ncei.noaa.gov/; accessed May 2024). Most of this winter precipitation is derived from a North Pacific Ocean source, as moist air masses move inland over the Sierra Nevada (e.g., Pyke, 1972; Cayan and Peterson, 1989). However, an increasing percentage of annual precipitation in California is derived from atmospheric rivers (AR) from the subtropical Pacific (Dettinger, 2011; Ralph and Dettinger, 2011), accounting for up to 50% of west coast precipitation in recent years (Dettinger, 2013), contributing to 22–73% of winter snowpack (Guan et al., 2010, 2013). A recent modeling study proposed that ARs will have an even greater role as the century continues, with overall precipitation and the potential for hazardous extreme events increasing (Rhoades et al., 2020). A consequence of this shift is that ARs will transition from largely beneficial to largely hazardous, especially as back-to-back AR events become more common (Rhoades et al., 2020). These shifts in precipitation source could lead to shifts in isotope values for the water entering June Lake, which could be captured in the carbonate geochemistry. Studies suggest that AR precipitation is isotopically depleted compared to non-AR storms (e.g., Peltier, 2023; Greenblat et al., 2024).

A number of data sets measured on different sample types were used in this study, including modern water samples, surface sediment samples, and sediments of a composite sediment core. Oxygen ($\delta^{18}O$) and hydrogen ($\delta^{2}H$) isotopes of water were measured to establish June Lake's position on the local evaporation line (LEL), and to track present moisture sources. These data were also needed to establish whether carbonate preserved in surface samples precipitates in equilibrium with modern lake water. The carbonate record from the sediment core was used to track hydroclimate changes and drought frequency over the Late Holocene, which we define here as the last ~4600 years, or the full span of our core record.

Methods

Surface water samples (n = 10) were collected from the shorelines of June Lake, Gull Lake, Reversed Creek, Silver Lake, and Rush Creek in September 2019 (Fig. 1). Sample containers were rinsed with lake or river water prior to sample collection, submerged, and capped underwater to minimize headspace and prevent in situ evaporation. $\delta^{18}O$ and $\delta^{2}H$ values for water samples were determined at the University of Kentucky's Stable Isotope Geochemistry Laboratory (KSIGL) using a Los Gatos Research T-LWIA-45-EP liquid water isotope analyzer. Raw data were normalized using USGS49 and USGS50 standards. In-session standard deviations for these standards were both <0.1‰. Duplicate measurements of each sample produced an average difference of 0.4‰ for $\delta^{2}H$ and 0.1‰ for $\delta^{18}O$. Final $\delta^{2}H$ and $\delta^{18}O$ values are expressed in ‰ relative to Vienna Standard Mean Ocean Water (VSMOW). Data from Waterisotopes.org were used for comparison with sampled waters and to develop global and local meteoric water lines (Bowen and Revenaugh, 2003; Bowen, 2011).

To determine if carbonate isotope values had variability within modern June Lake sediments, we collected surface sediment (upper ~1 cm) samples from a grid covering the lake floor (n = 36; Supplementary Fig. 1) using a Ponar grab sampler. To study changes in geochemistry through time, a pair of overlapping sediment cores, JUNE-JNE16-11A/B, were collected from a UWITEC percussion piston coring platform in 2016; details of the core collection and initial sampling procedures can be found in Lyon et al. (2020). Here, we increased the bulk-carbonate sample resolution in the composite core from the previous 5 cm resolution data set from Lyon et al. (2020) to ~2–3 cm, using the earlier data alongside the new.

Initial sediment characterization was based on smear slides, which were made following standard Continental Scientific Drilling (CSD) Facility procedures (Schnurrenberger et al., 2003; Myrbo, 2013) for all surface samples and a representative selection of core samples. Both sets of samples were measured for total inorganic carbon (%TIC) on a UIC Coulometrics CM5130 coulometer and those concentrations were used to determine the appropriate mass for isotopic measurements. Precision based on repeated measurements of a pure $CaCO_3$ standard was ≤0.11%. Samples with <0.17% TIC were omitted from gas bench measurements, as reliable isotopic data were not possible at such low carbonate concentrations.

The age model for core JUNE-JNE16-11A/B (Fig. 2) is from Lyon et al. (2020) and was based on 19 radiocarbon ages from both the JUNE-JNE16-11A/B and JUNE-JNE16-16 cores (Table 1; hereafter core 11 and core 16, respectively), correlated based on lithology and peaks in magnetic susceptibility, and the North Mono Tephra (Bursik and Sieh, 2013). Materials selected for radiocarbon dating were limited to plant macrofossils and charcoal, owing to the challenges in achieving accurate dates on other carbon-bearing materials (e.g., bulk sediment, carbonates) (e.g., Zimmerman and Wahl, 2020). The Bayesian statistical program "rbacon" (version 2.5.7; Blaauw and Christen, 2011) was used to model the age–depth relationship for the entire core at 0.1 and 0.5 cm, and at the bulk sampling resolution (2–3 cm) (Fig. 2).

To determine the relative abundance of different elements through time, core 11, which spanned a greater time interval than core 16, was analyzed on the University of Minnesota-Duluth's ITRAX XRF core scanner. Samples were measured at 5 mm intervals with a Cr-HE source, and at 1 mm intervals on a Cr source; both data sets were run with a 15 s dwell time. The analysis yielded semiquantitative major and trace elemental data for 36 elements in units of counts per second (cps). To further characterize mineralogy, dried and

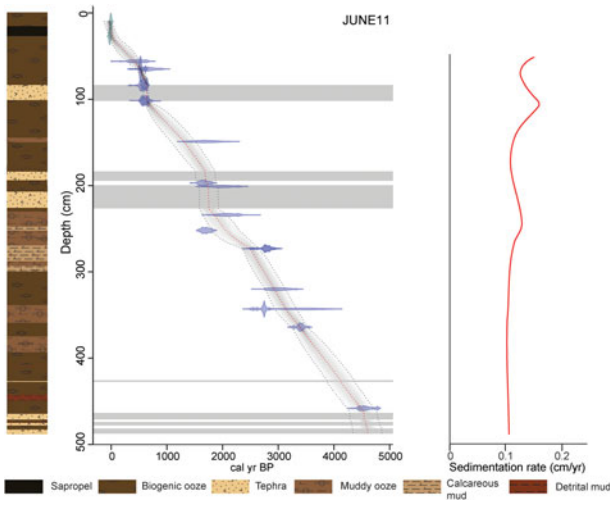

Figure 2. Left: Bacon age model results showing the width of the 95% uncertainty window for JUNE-JNE16-11A/B. Gray bands are tephras, which we interpret to represent near-instantaneous sedimentation. Right: The sedimentation rate in cm/yr for the same core. Note that the same y-axis is used for this panel and that the uppermost 50 cm are not included due to high water content, which would suggest an artificially high sedimentation rate.

https://doi.org/10.1017/qua.2024.38 Published online by Cambridge University Press

Table 1. Radiocarbon dates used to construct the age model for June Lake core 11. The model includes dates from another core in the same lake (core 16), which were interpolated for core 11 based on correlation using lithologic units and magnetic susceptibility, as described in Lyon et al. (2020)

CAMS #	Sample name	Sample description	Depth (cm)[a]	^{14}C age (years BP)	+/-	Fraction modern	+/-
177155	11A-1G-1, 23	Plant macrofossil fragments, minor arthropod parts	10	>Modern		1.0345	0.0057
180172	16A-1N-1_26	Plant-charcoal fragments	27	>Modern		1.3555	0.0352
180173	16A-1N-1_43	Plant-charcoal fragments	56	470	140	0.9431	0.0154
177852	11A-1U-1, 69-70, char	Aggregated charcoal	65	505	35	0.9390	0.0036
177853	11A-1U-1, 69-70, char	Plant macrofossil fragments	65	690	150	0.9176	0.0164
116694	16A-1N-1_62	Single plant macro (twig)	83	620	30	0.9259	0.0033
116693	16A-1N-1_77	Single plant macro (grass)	102	675	30	0.9194	0.0033
180347	11A-1U-2, 48-49	Charcoal, plant macrofossils	149	1760	190	0.8031	0.0185
116691	16A-1N-1_112	Plant-charcoal fragments	197	1750	60	0.8039	0.0050
176415	11A-2U-1, 25	Unspecified organic fragments	201	2010	160	0.7782	0.0152
180174	16A-2N-3_50	Plant-charcoal fragments	234	2110	130	0.7695	0.0119
177858	11A-2U-1, 64-65, char	Aggregated charcoal	252	1780	50	0.8014	0.0046
118244	16A-2N-3_73, char	Aggregated charcoal	273	2640	70	0.7200	0.0058
118245	16A-2N-3_73.5, macro	Plant macrofossil fragments	273	2680	70	0.7167	0.0055
180348	16A-2N-3_97.5	Charcoal, plant macrofossils	320	2850	130	0.7015	0.0113
177856	11A-2U-2, 54-55	Aggregated charcoal	343	2610	45	0.7226	0.0040
177857	11A-2U-2, 54-55, bugs	Arthropod parts, plant macrofossils	343	3250	220	0.6668	0.0180
177851	11B-2U-1, 29-30	Aggregated charcoal	364	3175	50	0.6737	0.0040
177156	11B-2U-2, 47	Charcoal, plant macrofossils	458	4050	60	0.6040	0.0042

[a]Depth in cm is for core 11.

powdered samples were scanned using a Diano 2100-E X-ray diffraction (XRD) instrument with a copper target. Peaks of the important carbonate minerals were identified by comparison with known minerals from the RRUFF database (Lafuente et al., 2016).

Sediment samples for carbonate isotope analyses were pretreated with 2.5% bleach followed by multiple rinses with deionized water to remove organic carbon using the CSD standard operating procedure for lake sediment decarbonation (https://cse.umn.edu/csd/subsample-preparation-and-analysis; accessed July 2024). Samples were then dried in either a low temperature oven (45°C for 48 hours) or a freeze-dryer. Following the KSIGL gas bench standard operating procedure, dried carbonate samples were loaded into acid-cleaned 12 mL Exetainers and dried overnight at 70°C to remove adsorbed water. Each Exetainer was then sealed with a septum cap and flushed with ultra-high purity (99.999% pure) He for 12 minutes to remove atmospheric N_2 and CO_2. Following the He flush, 0.1 mL of dewatered H_3PO_4 (final concentration 104%) was injected through the septum and allowed to react with the sample for at least 24 hours at 25°C to produce CO_2. Seven consecutive aliquots of headspace gas from each Exetainer were transferred via autosampler to a Thermo GasBench II interfaced with a Thermo Finnigan DELTAplus XP isotope ratio mass spectrometer for measurement. Uncorrected oxygen and carbon isotope values were normalized to Vienna Pee Dee Belemnite (VPDB) using at least two internationally certified reference materials with contrasting $\delta^{18}O$ and $\delta^{13}C$ values: NIST 915b ($\delta^{18}O = -23.4$, $\delta^{13}C = -8.6$), NBS-18 ($\delta^{18}O = -23.2$, $\delta^{13}C = -5.01$), and NBS-19 ($\delta^{18}O = -2.2$, $\delta^{13}C = 1.95$) (after Coplen et al., 2006). Blind standards were analyzed to assess precision and accuracy. Duplicates of unknowns were also analyzed to assess the reproducibility of measurements. The precision and accuracy of the $\delta^{18}O$ data were assessed with multiple in-session measurements of NIST-915b; both values were <0.4‰. The precision and accuracy of the $\delta^{13}C$ data, assessed in the same manner, were both 0.2‰. The reproducibility of $\delta^{18}O$ and $\delta^{13}C$ data, assessed with sample duplicates, were 0.2 and 0.1‰, respectively.

We matched horizons from the 5 mm Ca/Ti data set to the lower resolution (2–3 cm) %TIC data sets by applying a five-point running average to the 5 mm XRF data and only compared those depths for which we also had bulk geochemical data. We used the program PAST (Paleontological Statistics Software; Hammer et al., 2001) to apply LOESS filters to the carbonate isotope chemostratigraphic data, which is a line of best fit through a data distribution that allows for visualization of relationships between measured variables and time. We use the resulting LOESS curves

https://doi.org/10.1017/qua.2024.38 Published online by Cambridge University Press

to interpret non-parametric temporal trends. We also analyzed correlations among measured indicators using linear regression analysis with PAST.

Results

Water isotopes

June Lake surface waters have $\delta^{18}O$ values of −2.7 to −3.9‰ and $\delta^{2}H$ values of −55.1 to −53.9‰, similar to published values of −3.3‰ and −59.6‰ for June Lake water collected in September 2007 (Brooks et al., 2014). Isotope values for surface waters in the study area were lowest in the most downstream reaches (Reversed and Rush creeks) and highest in June Lake, the only closed lake basin in our transect (Table 2, Fig. 1). These water isotope values were plotted against the global meteoric water line (Fig. 3). June and Gull lakes are isotopically heavier than average regional precipitation, but the streams and Silver Lake are lighter (Fig. 3). Our water samples were collected in September 2019, a time of year when isotopic values for precipitation (−9.5‰ and −66‰ for $\delta^{18}O$ and $\delta^{2}H$, respectively; Bowen and Revenaugh, 2003; Bowen, 2011) are greater than average (avg = −12.2‰ and −88.7‰ for $\delta^{18}O$ and $\delta^{2}H$, respectively) due to warm late summer water temperatures in the source area and higher condensation temperatures (e.g., Dansgaard, 1964).

Snowmelt charged streams entering Mono Lake from the Sierras range from −15.8 to −13.8‰ for $\delta^{18}O$ (Li et al., 1997). Mono Lake water was measured at −0.1‰ ($\delta^{18}O$) at Navy Beach along the southern shore (Li et al., 1997). An early study by Friedman et al. (1964) recorded a $\delta^{2}H$ of −6.2‰ for Mono Lake, but more recent $\delta^{2}H$ values for Mono Lake water are unavailable.

Table 2. Water isotope values from waterbodies in the study area. All are measured in per mil, relative to Vienna Standard Mean Ocean Water

Site name	Location details	$\delta^{18}O$	$\delta^{2}H$
June Lake	Northeast shoreline	−2.8	−55.1
		−2.7	−54.2
June Lake	Northeast shoreline	−2.8	−54.3
		−2.9	−54.3
June Lake	Northeast shoreline	−2.8	−54.1
		−2.8	−54.0
June Lake	Northwest shoreline	−2.7	−53.9
		−2.8	−54.0
June Lake	Southeast shoreline	−3.9	−59.6
		−3.8	−59.7
June Lake Average		**−3.0**	**−55.3**
Gull Lake	Northern shoreline	−9.9	−91.6
		−9.8	−91.6
Gull Lake	Reversed Creek outlet	−9.6	−91.4
		−9.6	−91.2
Gull Lake Average		**−9.7**	**−91.4**
Gull Meadow	Marsh west and north of Gull Lake	−16.4	−124.4
		−16.3	−123.4
Reversed Creek	Between Gull and Silver lakes	−15.7	−118.4
		−15.8	−118.6
Silver Lake	Western shoreline	−15.0	−111.8
		−14.8	−111.3
Rush Creek	Between Silver and Grant lakes	−15.2	−113.9
		−15.2	−113.4
Average for streams and Silver Lake		**−15.3**	**−114.6**
Average for all waterbodies		**−8.8**	**−84.3**
Standard deviation for all data		**5.8**	**28.7**

Sediment composition and sedimentation rate

Modern surface sediments

Surface sediments from June Lake are primarily diatomaceous oozes, particularly in the two depocenters (Fig. 1; Lyon et al., 2019). $\delta^{18}O_{carb}$ and $\delta^{13}C_{carb}$ values (Table 3) are generally lower in the two deepwater depocenters than in shallower areas of the lake (Lyon et al., 2019). In particular, $\delta^{18}O_{carb}$ values are lowest in areas where water depth exceeds 30 m (Fig. 4), and values are highest closest to the shoreline. For $\delta^{13}C_{carb}$, values are highest (>2.0‰) at the shallow, northeastern beach (Fig. 4). In contrast, $\delta^{13}C_{carb}$ values are lowest (<1.0‰) in the deepwater just offshore of this beach, and in the southwestern depocenter. Carbonate isotope values for surface sediments are weakly correlated ($R^2 = 0.18$; Supplementary Fig. 2).

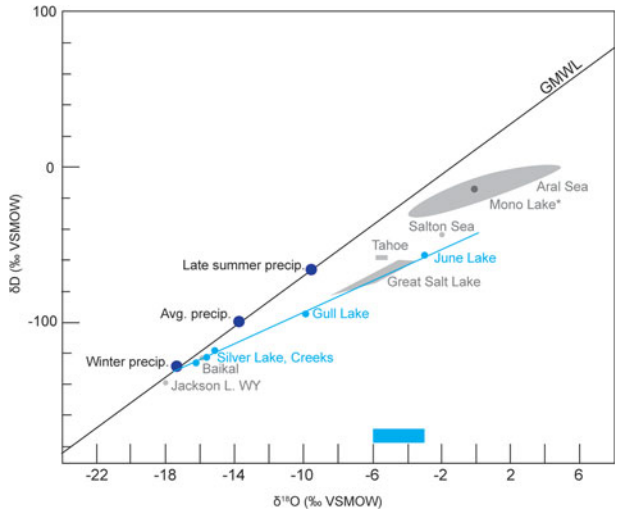

Figure 3. Cross plot of average water isotope values in per mil for waterbodies in the study area (light blue dots) and selected global and regional lakes (gray dots and polygons). Standard deviations for these values are 0.45 and 2.32 for June Lake, 0.15 and 0.19 for Gull Lake, and 0.39 and 3.20 for $\delta^{18}O$ and $\delta^{2}H$, respectively. The global meteoric water line (GMWL) is also shown for reference (after Jasechko et al., 2013). Large, dark blue dots on the GMWL mark values for precipitation in the June Lake region. An evaporation line for the study area is shown in light blue with a shallower slope than the GMWL. The blue horizontal bar along the x-axis shows the range of surface sediment $\delta^{18}O$ values in June Lake. *Mono Lake values (Friedman et al., 1964; Li et al., 1997) represented by dark gray circle within Aral Sea polygon.

https://doi.org/10.1017/qua.2024.38 Published online by Cambridge University Press

Table 3. Surface sediment carbonate isotope values. All are measured in per mil, relative to Vienna Pee Dee Belemnite

Sample	$\delta^{18}O$	$\delta^{13}C$
F002	−3.9	3.7
F004	−5.9	1.6
F005	−5.1	2.2
F006	−5.8	2.1
F007	−6.0	1.6
F011	−3.7	2.4
F012	−5.9	1.5
F013	−5.6	1.7
F014	−6.1	1.7
F016	−5.5	1.7
F017	−5.6	1.5
F019	−5.4	1.3
F020	−4.5	1.7
F023	−5.2	0.9
F025	−4.0	1.4
F026	−4.6	0.8
F027	−5.2	0.7
F028	−4.9	0.9
F029	−5.8	0.8
F032	−5.3	0.6
F033	−5.2	0.7
F034	−5.0	0.9
F035	−3.9	1.2
JL16-005	−3.2	2.1
JL16-012	−4.4	1.2
JL16-013	−4.7	0.9
JL16-014	−3.6	2.0
Jl16-015	−3.4	2.2
JL16-017	−3.3	2.4
JL16-018	−5.3	1.2
JL16-019	−5.2	1.2
JL16-020	−5.2	1.2
JL16-021	−5.4	0.4
JL16-022	−4.1	2.4
JL16-025	−4.7	1.6
JL16C-2	−5.3	1.4
JL16C-3	−5.3	1.4
Average	**−4.9**	**1.5**

Core sediments

Lyon et al. (2020) established the sedimentology and stratigraphy of the June Lake cores as algae-rich oozes, with intervals of muddy ooze and carbonate mud (Fig. 2). Seven distinct tephras punctuate the stratigraphy, and in some cases, provide distinct chronological controls. Smear slide analysis allowed us to establish the dominant carbonate mineralogy as calcite. Most of the calcite was small (<10 mm), sub-equant crystals (Lyon et al., 2020). Ostracods were observed in some horizons while subsampling, but smear slide analysis reveals them to be a minor component overall, so we were largely able to avoid them in bulk sampling. Further, their shells are composed of low Mg-calcite (e.g., Holmes and De Deckker, 2012), which is consistent with the dominant carbonate mineralogy established in smear slide analysis (Lyon et al., 2020). Dolomite and aragonite were both very rare in the smear slide analysis. XRD peaks for horizons with high %TIC were identified at 29.4, 47.6, and 48.6 degrees 2-theta (Supplementary Fig. 3). We focus on further interpreting the mineralogy of the carbonate sediments and their utility as hydroclimate indicators in the "Discussion".

Excluding the tephras, which represent near-instantaneous deposition, the sedimentation rate in June Lake is relatively constant (∼1 mm/yr) throughout the core, with a higher apparent rate in the uppermost, waterlogged part of core 11 (Fig. 2). The 95% uncertainty envelope for most of the age–-depth model produces an uncertainty range of less than 200 years around any given depth in the core. However, some areas, including the middle and bottom sections of the core, have uncertainties closer to 240 years (Table 4). Age model results are described in greater detail in Lyon et al. (2020). Both the %TIC and carbonate isotope values (sampled every 2–3 cm) are lower resolution than the high-resolution (0.1 cm) XRF record. The sampling for carbonate isotope analysis used ∼1 cm^3, and thus each sample integrates ∼10 years based on the overall sedimentation rate, whereas each XRF data point represents ∼1 year based on the same rate. Thus, we feel confident that our record provides centennial-scale resolution or better.

The sediment geochemistry record over the last 4600 years includes several centennial intervals of elevated %TIC (Fig. 5). Six prominent %TIC peaks appear, centered on ∼3700, 3200, 2500, 2000, 1100, and 70 cal yr BP. Alongside many of these broad peaks are numerous discrete multidecadal peaks in the 1 mm Ca/Ti data set (1–18 in Fig. 5). For example, two %TIC peaks at ∼2500 and 2670 cal yr BP occur within an extended period of elevated carbonate accumulation from 2900 to 2440 cal yr BP; the Ca/Ti curve defines two distinct peaks from 2740 to 2670 and 2530 to 2430 cal yr BP, after which time Ca/Ti values decline, but remain relatively high until about 2330 cal BP. We designated Ca/Ti values greater than 56 (2-sigma deviation) as peaks in that indicator. The exception to this is the most recent part of the record, in which Ca/Ti count values approach, but do not exceed, 56. The Ca/Ti curve shows higher frequency variability throughout the core than the %TIC data, albeit with similar overall structure.

Values for $\delta^{18}O_{carb}$ and $\delta^{13}C_{carb}$ range from −13.6 to −4.4‰ and −1.2 to 2.7‰, respectively. Although this data set is lower resolution than the scanning XRF-derived Ca/Ti data, the long-term trends share many similarities. Higher carbonate isotope values tend to co-occur with each other and occur at the same times as the peaks in %TIC and Ca/Ti, though with offsets due to the different sample resolution. One example of this disparity occurs at ∼3200 cal yr BP. In the Ca/Ti data, this interval of elevated values is separated into two prominent peaks centered at 3170 cal yr BP and 3110 cal yr BP, respectively (Table 4).

https://doi.org/10.1017/qua.2024.38 Published online by Cambridge University Press

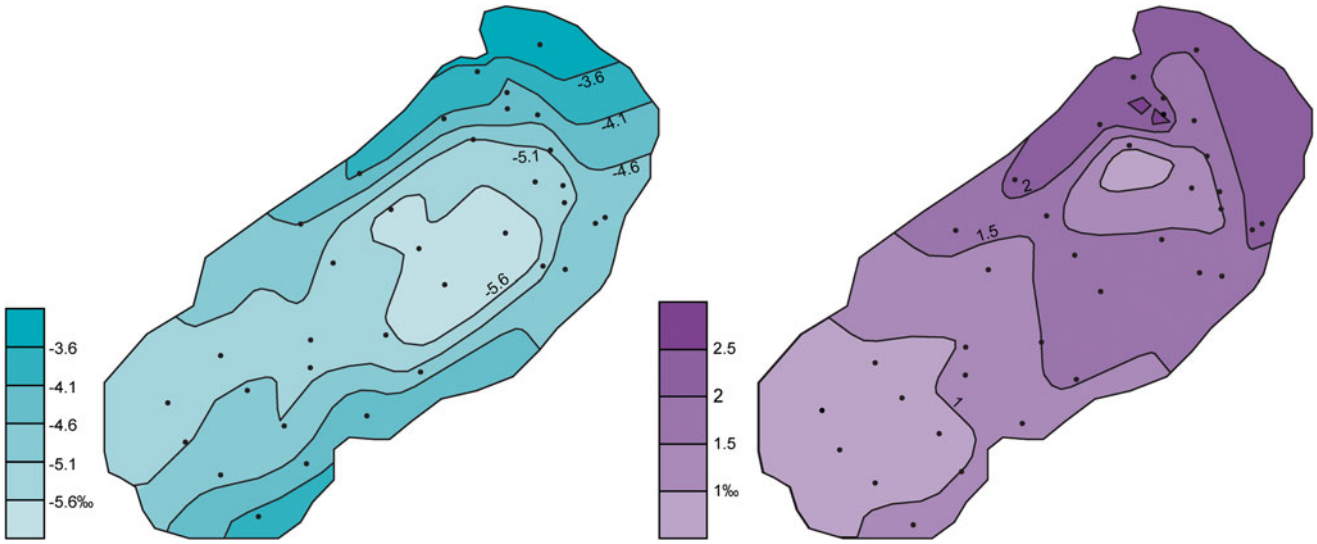

Figure 4. Carbonate isotope values for surface sediments in June Lake. Each black dot represents a sample location on the lake floor. Left: $\delta^{18}O_{carb}$ values. Right: $\delta^{13}C_{carb}$ values.

Discussion

Water isotopes

To determine the viability of $\delta^{18}O$ as a proxy for the ratio of precipitation to evaporation (P/E), we considered the difference between the isotopic values of lake water and meteoric water in the study area, including the presumed termination of the flow path at Mono Lake. We applied the water isotope values ($\delta^{18}O$ and $\delta^{2}H$) for June Lake and the other waterbodies in Figure 1 to determine June Lake's position on the LEL (Fig. 3). Although June Lake water is isotopically heavier than regional precipitation, Rush Creek, Reversed Creek, Silver Lake, and Gull Lake are lighter likely due to the "catchment effect" wherein the water in the streams is lighter due to the direct contributions of upstream snowmelt and precipitation (Friedman et al., 1992). These data are valuable for discriminating isometer type at June Lake: a precipitation isometer (recording precipitation $\delta^{18}O$), a P/E isometer (where $\delta^{18}O$ values reflect both precipitation and fractionation by evaporation), or a terminal basin, where all water loss is by evaporation and the $\delta^{18}O$ of lake water is most strongly influenced by evaporative fractionation and is therefore very high compared to the other two systems (after the model of Anderson et al., 2016).

The likeliest terminal basin under the Anderson et al. (2016) model in the study area is Mono Lake (Fig. 1). However, published water isotope values for Mono Lake ($\delta^{18}O = -0.1‰$ and $\delta^{2}H = -6.2‰$; Friedman et al., 1964; Li et al., 1997) suggest that it is not along the same evaporation trend as the other waterbodies and thus not the endmember of the LEL defined by the waters in the study area (Fig. 3). This is not entirely unexpected, since Mono Lake has a much larger and geologically more variable watershed (John et al. 2012) than the study area, and has many faults and springs through which hydrothermal water or deep ground water likely enters the lake, disconnecting it geochemically from meteoric waters (Oremland et al. 1987; Tomascak et al. 2003). Based on our water isotope data, June Lake would thus seem to be the endmember of the LEL for the waterbodies studied, which would make it a terminal basin as opposed to a P/E isometer in the Anderson et al. (2016) model. However, there remains a question of whether June Lake is hydrologically open in the subsurface, and by consequence a P/E isometer.

June Lake has the highest water isotope values of all the waterbodies we measured (averages: $\delta^{18}O$ −3.0‰ and $\delta^{2}H$ −55.3‰; Table 2, Fig. 1), which is interpreted to be a consequence of seasonal evaporative concentration. Gull Lake, despite having a surface outlet, has notably higher isotope values (averages: $\delta^{18}O$ −9.7‰ and $\delta^{2}H$ −91.4‰; Table 2, Fig. 1) than the other open lakes and streams we measured. One potential explanation for this unexpected isotopic composition is subsurface seepage of water from June Lake into Gull Lake, notionally following flow paths through the marsh that separates the basins (Fig. 1). We hypothesize that Gull Lake's intermediate isotopic composition results from a mixture from water sources with varied isotopic composition: direct precipitation, seasonal runoff from snowmelt, and contributions of seepage from June Lake, suggesting that June Lake is not entirely hydrologically closed. This interpretation supports the idea that June Lake is a P/E isometer rather than a terminal basin. Carbonate isotope values from core sediments described below provide additional context for our ability to interpret June Lake's status as a P/E isometer.

Carbonate mineralogy and its utility as a hydroclimate indicator

Establishing dominant carbonate mineralogy

Smear slide analysis (Lyon et al., 2020) suggests the dominant carbonate mineralogy in the core is calcite. New XRD data from this study confirm that interpretation; the dominant peak for most samples is at approximately 29.4° 2-theta, consistent with diffractograms of calcite reference materials, and smaller peaks at 47.6° and 48.6° 2-theta are also indicative of calcite (Supplementary Fig. 3). This is important to note, as other carbonate phases, such as dolomite, require correction with a different fractionation factor for $\delta^{18}O_{carb}$ and $\delta^{13}C_{carb}$ values if present (e.g., McCormack and Kwiecien, 2021).

https://doi.org/10.1017/qua.2024.38 Published online by Cambridge University Press

Table 4. Times of increasing carbonate precipitation from the June Lake carbonate archive as designated from rising limbs of Ca/Ti curve. Age model 95% uncertainty is reported for each drought depth. Drought midpoint reported as median years in cal yr BP, rounded to the nearest 10. The average time between intervals of increasing carbonate accumulation is ~230 years

Core depth of drought midpoint	Age model 95% uncertainty at midpoint depth	Approx. drought midpoint in years	Approx. drought duration in years	Time between droughts in years	Drought number used in Fig. 5	Associated drought (named)[a]
10.15	40	−30			20	Modern
121.15	180	890	20	920	19	MCA
143.10	220	1220	40	330	18	MCA
228.50	190	1790	20	570	17	
237.45	200	1900	30	110	16	
240.90	220	1940	10	40	15	
247.65	230	2020	20	80	14	LHDP
254.35	240	2110	10	90	13	LHDP
257.10	240	2170	20	60	12	LHDP
260.55	230	2240	30	70	11	LHDP
274.65	180	2520	40	280	10	LHDP
292.80	190	2670	20	150	9	LHDP
323.65	180	2950	10	280	8	
342.05	190	3120	30	170	7	LHDP
347.30	180	3180	10	60	6	LHDP
371.30	170	3460	10	280	5	early LHDP?
383.40	210	3600	20	140	4	
386.70	210	3640	20	40	3	
413.60	250	3950	20	310	2	
455.65	240	4440	20	490	1	

[a]MCA, Medieval Climate Anomaly; LHDP, Late Holocene Dry Period.

Determining whether calcite precipitates in equilibrium with lake water

To determine whether June Lake carbonates precipitate in equilibrium with lake water, we applied Leng and Marshall's (2004) equation to values for oxygen isotopes in both June Lake water (δw) and surface sediment samples (δc):

$$T^{\circ}\mathrm{C} = 13.8 - 4.58(\delta c - \delta w) + 0.08(\delta c - \delta w)^2$$

Using a value of −2.8‰ for δw (June Lake $\delta^{18}O_{water}$) and a T of 11.5°C (surface water temperature when samples collected in early fall), we calculated δc ($\delta^{18}O_{carb}$) = −5.0‰, which is approximately the average value for surface sediments (−4.9‰; Table 3). Thus, it is likely that carbonates precipitate at or near equilibrium conditions with the lake water. While some researchers (e.g., Daeron et al., 2019) suggest such a validation step is superfluous given the likelihood that most calcites are in disequilibrium from the host waters, this does not appear to be the case at June Lake. This validation of equilibrium precipitation adds confidence to our interpretation of the $\delta^{18}O_{carb}$ record as one of hydroclimatic change.

Establishing the Ca/Ti record as one of carbonate accumulation

There is a relatively strong correlation between %TIC and Ca/Ti (Fig. 6; $R^2 = 0.68$; P value < 0.00001 at 0.05 significance threshold); it is important to note that the peak heights are greater relative to baseline values for the Ca/Ti record than for the %TIC, which may make this correlation weaker than the depth match in peaks would suggest. Nonetheless, the correlation suggests that most Ca is bonded to the carbonate ion as calcite, rather than another mineral phase such as gypsum or anhydrite, neither of which were observed on smear slides or on X-ray powder diffractograms. From these tests we conclude that Ca/Ti reliably approximates $CaCO_3$ in Late Holocene-age June Lake sediments. This application is consistent with several other lake sediment studies (e.g., Kylander et al., 2011; Liu et al., 2013; Davies et al., 2015).

Using carbonate isotope geochemistry to determine June Lake hydrology

Large, hydrologically closed lakes tend to have strong correlations between $\delta^{13}C_{carb}$ and $\delta^{18}O_{carb}$ ($R^2 > 0.7$), whereas open lakes have a weaker correlation and a narrower range of $\delta^{18}O$ values (Talbot, 1990; Talbot and Kelts, 1990). Despite high covariance between $\delta^{18}O$ and $\delta^{13}C$ when carbonate content is high (e.g., $R^2 = 0.83$, $P < 0.05$ during peaks of Zone D of Figure 5, discussed below), for the June Lake core record, the overall R^2 is 0.32, which is consistent with an open hydrology, whereas times of higher correlation are interpreted as more closed to surface outflow. Further, the low correlation in modern June Lake sediments ($R^2 = 0.18$) supports open hydrology following the Talbot (1990) and Talbot and Kelts (1990) model.

This lack of isotopic covariance may be due to the subsurface seepage out of June Lake, so we cannot reliably use the core record of isotopic covariation (Fig. 6A) as a proxy for changes in the

https://doi.org/10.1017/qua.2024.38 Published online by Cambridge University Press

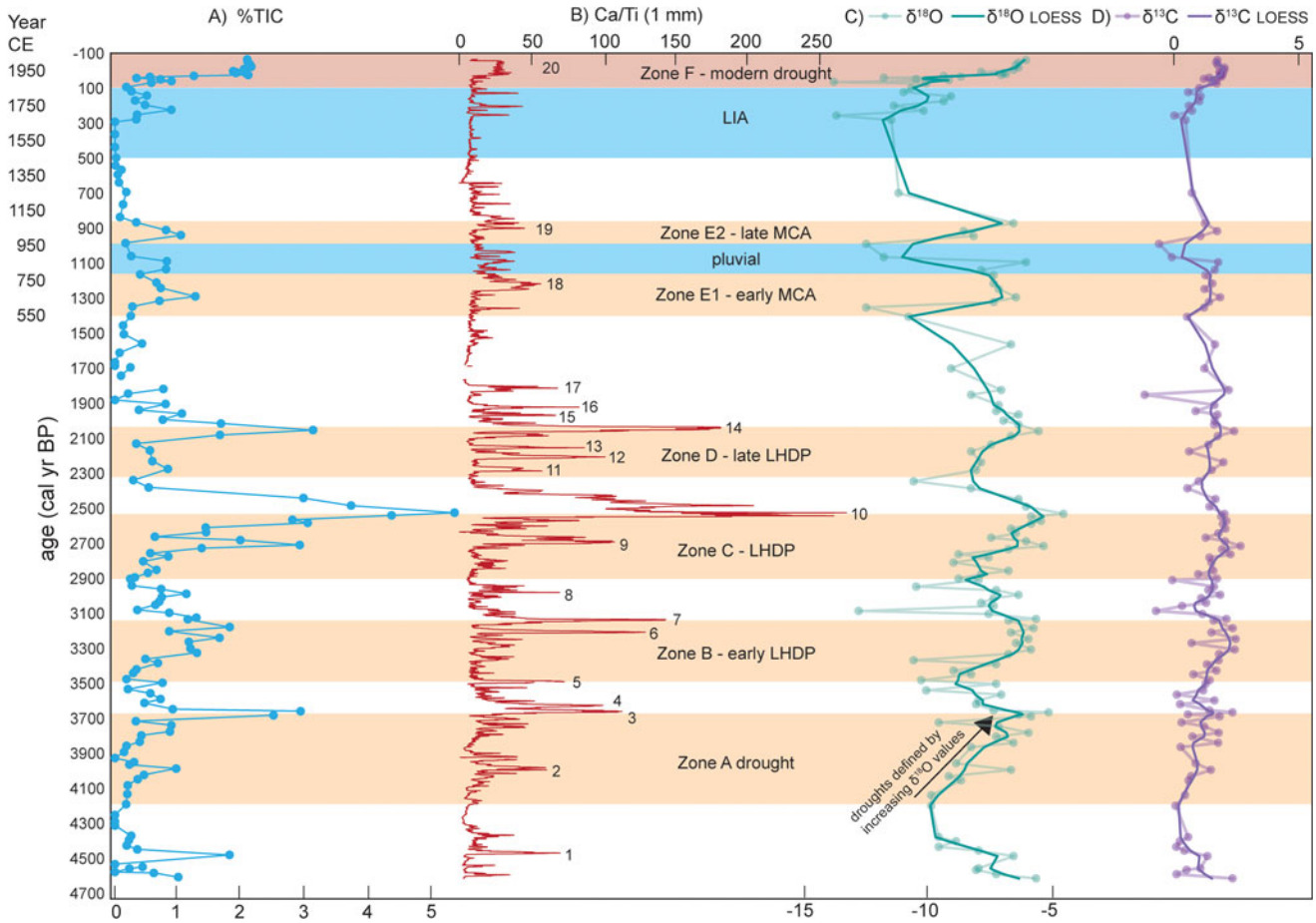

Figure 5. Plot of changes in core geochemistry with time. From left to right: (A) total inorganic carbon (%TIC), sampled every 2–3 cm; (B) ratio of calcium to titanium (Ca/Ti), sampled every 1 mm; (C) oxygen isotope values in per mil ($\delta^{18}O_{carb}$), sampled every 2–3 cm where %TIC was high enough to permit measurement; (D) carbon isotope values in per mil ($\delta^{13}C_{carb}$), sampled every 2–3 cm where %TIC was high enough to permit measurement. A LOESS smoother applied to the $\delta^{18}O$ and $\delta^{13}C$ data sets (heavy lines) shows broader changes through time. Here, the six dry intervals described in the text are particularly prominent as increases in oxygen isotope values—these are denoted by horizontal yellow or red bars. The horizontal blue bars indicate the wetter intervals, including the pluvial between the two peaks of the Medieval Climate Anomaly (MCA) megadrought and the Little Ice Age (LIA) (~500–100 cal yr BP, as defined in IPCC, 2021). LHDP, Late Holocene Dry Period.

surface connectivity between June and Gull lakes over the Late Holocene. Instead, we focus on interpreting hydroclimate changes over time using Ca/Ti and $\delta^{18}O_{carb}$.

Reconstructing hydroclimate with carbonate core sediments

We interpret both the bulk sedimentary %TIC and high-resolution Ca/Ti data as a response to changes in P/E and lake level: When lake levels fall in response to decreasing precipitation or higher evaporation, calcite precipitates in response to the higher saturation state (e.g., Kelts and Hsü, 1978).

Variations in $\delta^{18}O$ in sediment records are also often interpreted as changes in the balance between precipitation and evaporation (e.g., Horton et al., 2015; Anderson et al., 2016). When evaporation is higher, the lighter ^{16}O preferentially evaporates, leaving water with a higher ratio of $^{18/16}O$ available during carbonate formation. We interpret such intervals in June Lake sediments as episodes of drought and resulting lake level low stands. In contrast, when effective moisture is higher, the P/E ratio is greater, lake levels are higher, and $\delta^{18}O_{carb}$ values are lower. The June Lake $\delta^{18}O_{carb}$ range is almost 10‰ over the period of record; this would represent at least a 30°C temperature change, which is highly unlikely, lending further support to the interpretation that $\delta^{18}O$ values are tracking P/E.

By applying a LOESS filter to the carbonate isotope data set, six broad dry periods interpreted from the rising limb of the $\delta^{18}O$ LOESS curve are apparent (Zones A–F in Fig. 5). In each of those dry periods, all other carbonate indicators are elevated (Fig. 5). Those six dry periods are described in greater detail below.

Whereas the bulk geochemical indicators (%TIC and $\delta^{18}O_{carb}$) reveal broad intervals of drought, the Ca/Ti data set has the capacity to resolve more discrete drought intervals either within or in addition to these periods (Table 4). We designated Ca/Ti values greater than 56 (2-sigma deviation from the average value) as peaks in carbonate accumulation corresponding to drought. The exception to this is the most recent part of the record, in which Ca/Ti values approach, but do not exceed, 56. For example, we find two consecutive Ca/Ti peaks suggesting short-duration droughts around the end of Zone A (peaks 3 and 4, Fig. 5), as well as two droughts separated by about a hundred years at the end of Zone B. Further, the Ca/Ti data set makes it clear that the response of the carbonate system tends to be abrupt, with carbonate precipitation taking place over a

https://doi.org/10.1017/qua.2024.38 Published online by Cambridge University Press

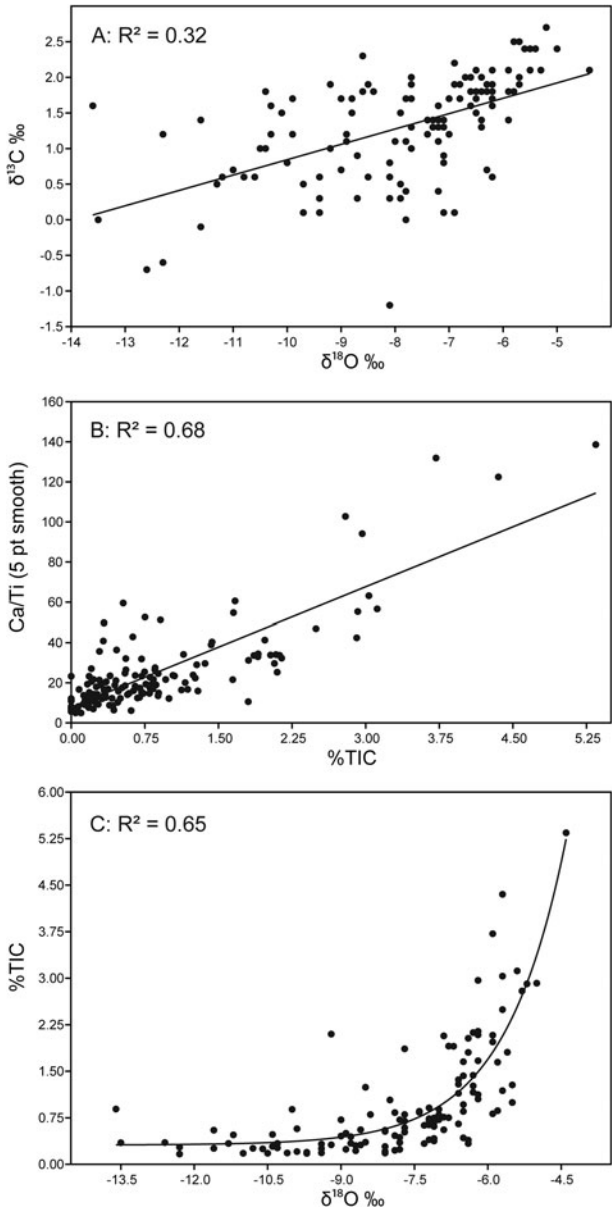

Figure 6. (A) Scatterplot of carbonate isotope values for core sediments from June Lake. The strength of this correlation is often used as an indicator of hydrologic closure (e.g., Talbot and Kelts, 1990). *P* value < 0.00001 at 0.05 significance threshold. (B) A strong positive correlation between %TIC and Ca/Ti for core sediments suggests most calcium is associated with an authigenic carbonate phase rather than detrital input, and may therefore be used as a proxy for %TIC in our high-resolution XRF data set. Owing to the differences in sampling resolution, we used a five-point running average on the Ca/Ti data set to ensure comparison of approximately the same strata for the two data sets. *P* value < 0.00001. (C) Scatterplot of $\delta^{18}O$ values and %TIC throughout the core. A logarithmic curve defines the relationship between these two indicators. *P* value < 0.00001. At %TIC values < ~1%, a range of low $\delta^{18}O$ values are possible (−13.5 to −6.5). However, when carbonate precipitation is greater (%TIC > 1), oxygen isotope values, though higher, are less variable (−6.5 to −4.4).

matter of years to decades following drought onset. During the LHDP, Ca/Ti peaks suggest the potential for seven episodes of drought, each separated by at least 50 years, with an average of 110 years between droughts (Table 4, peaks 6–14 in Fig. 5). In the intervening years, Ca/Ti counts return to values observed in wetter parts of the record.

Regional paleoclimate as interpreted from the June Lake carbonate record

The four hydroclimate zones established in Lyon et al. (2020) are described here to offer contrast with the findings of this study (Supplementary Fig. 4). The earliest of these zones (~4600–3600 cal yr BP) was a relatively wet interval, as demonstrated by high values for organic geochemical indicators, low % TIC, and several sand beds that suggested enhanced runoff. The second zone (~3600–1700 cal yr BP), which overlaps with the LHDP described by Mensing et al. (2013), is characterized by elevated carbonate precipitation and low algal production as indicated by organic carbon and biogenic silica. The third zone (~1700 cal yr BP to ~130 years ago) roughly corresponds with the relatively cold and wet Little Ice Age (LIA), though the early part also includes the MCA, which is characterized by two centennial-scale droughts interrupted by a pluvial interval. The youngest zone encompasses the last ~130 years (Current Warm Period) and is characterized by an abrupt decline in algal production, high %TIC, and a dramatic change in the diatom community that is consistent with a shift to enhanced stratification and warmer lake water (Streib et al., 2021). In the following sections, we describe the dry intervals that are better elucidated by our new carbonate data sets.

The Late Holocene Dry Period (~3200–1800 cal yr BP)

The most striking examples of drought in this record are the three zones (B–D in Fig. 5) exhibiting pronounced peaks in Ca/Ti between ~3500 and 2000 cal yr BP (Fig. 5). These zones likely represent the LHDP first described in Mensing et al. (2013) from Stonehouse Meadow (eastern Nevada) pollen and geochemistry records. The LHDP is partially correlative to the Marina Lowstand in Mono Lake (Stine, 1990; Zimmerman et al., 2021), and has been recognized in other areas of the Great Basin (e.g., Mensing et al., 2004, 2023; Theissen et al., 2019), the transitional area between the Great Basin and Colorado Plateau (Anderson et al., 2023), and southern California (e.g., Kirby et al., 2014, 2019), showing that the climatic drivers of the LHDP affected a broad region. A Great Basin drought beginning at ~3100 cal yr BP was identified in Millar et al. (2019) and was also identified as the initiation of the LHDP in Mensing et al. (2023). Our ~3200 cal yr BP droughts (peaks 6 and 7 in Fig. 5) are likely the same event, as the discrepancy is within the uncertainty of our radiocarbon age model (as well as those of the other sediment records). However, the June Lake record is more highly resolved than many of those other records (e.g., Mensing et al., 2013; Theissen et al., 2019), suggesting higher frequency drought variations within the dry "period" (Fig. 7).

Our record also shows the LHDP was likely not one continuous dry period, consistent with the observation of Mensing et al. (2023) that there were two droughts separated by a pluvial. Our record further resolves the LHDP into a series of discrete multidecadal drought episodes with decades to centuries separating each peak (peaks 5–14 in Fig. 5). Comparing the Ca/Ti data to the LOESS curve in Figure 5 shows this difference in resolution: Whereas the $\delta^{18}O$ LOESS curve shows broad intervals of low lake level and dry paleoclimate, the Ca/Ti curve resolves several discrete droughts over the same time periods. Thus, our record is distinct from many other LHDP records (and hydroclimate records from the region more generally) in that we can resolve many discrete droughts within the broader dry period. Wetter intervals may be present in other basins but partially obscured

https://doi.org/10.1017/qua.2024.38 Published online by Cambridge University Press

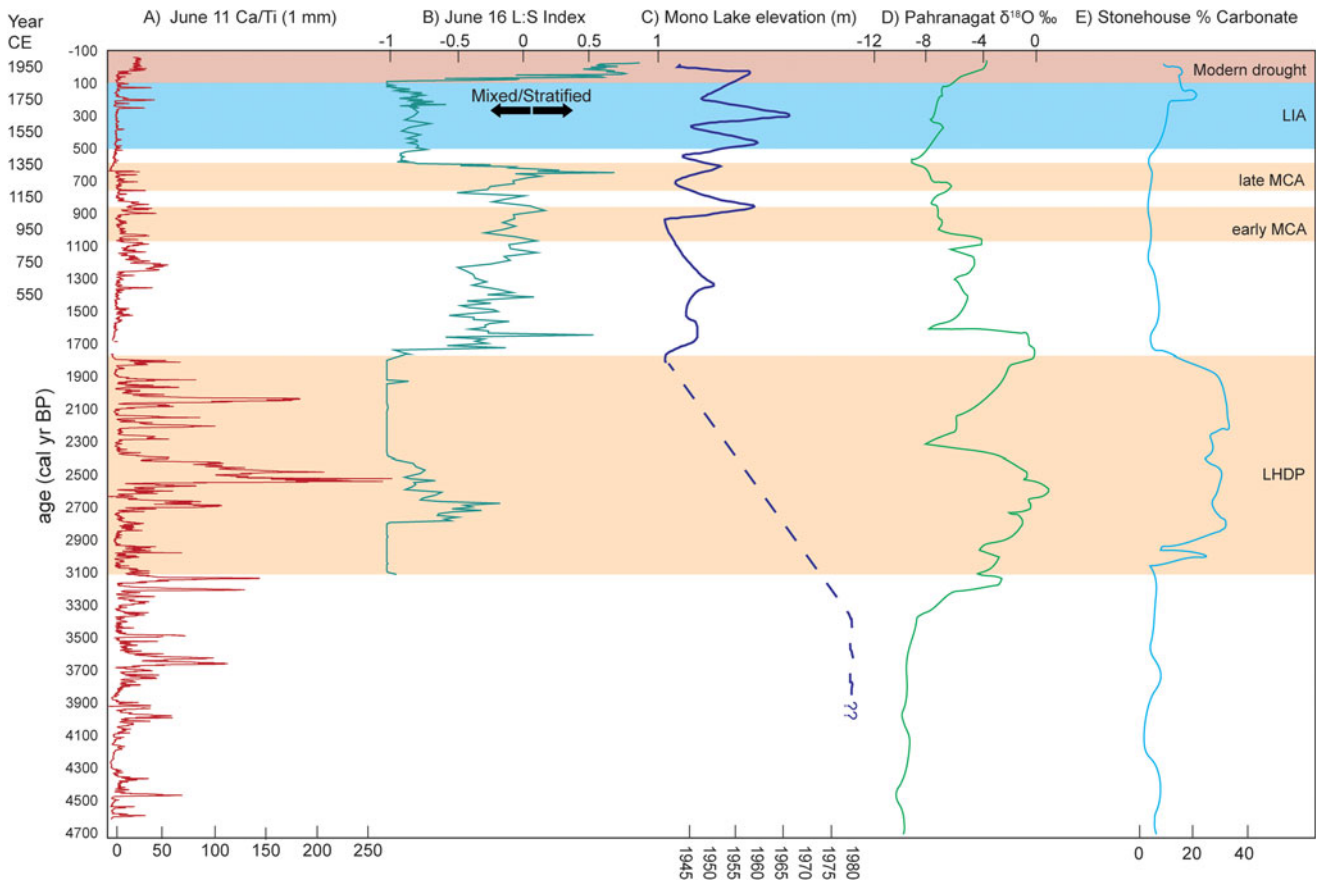

Figure 7. Great Basin regional records of hydroclimate change. (A) June Lake Ca/Ti data from core 11 (1 mm resolution—this study). (B) Ratio of *Lindavia*:*Stephanodiscus* diatoms from June Lake (Streib et al., 2021). (C) Mono Lake shoreline elevation (Stine, 1990). (D) $\delta^{18}O$ data for Pahranagat Lake from Thiessen et al. (2019). (E) %Carbonate from Stonehouse Meadow from Mensing et al. (2013). Horizontal bars defined using Mensing et al. (2023) (Late Holocene Dry Period [LHDP]), Stine (1994) (Medieval Climate Anomaly [MCA]), IPCC (2021) (Litte Ice Age [LIA]), and Streib et al. (2021) (modern drought).

by the proxy resolution, as in the Lyon et al. (2020) records—for example, Lake Pahranagat records a wet interval within the LHDP centered on 2350 cal yr BP (Theissen et al., 2019). The LHDP is characterized by drier than average conditions from ~3100 to 1800 cal yr BP (Millar et al., 2019; Mensing et al., 2023), but our record shows that there were also wet phases, in evidence from the high variability in carbonate abundance. It is possible that these wet phases were not sufficiently long enough to allow recovery of the ecosystems responding to the prolonged drought (e.g., Mensing et al., 2013, 2023; Millar et al., 2019), but were sufficiently wet to raise lake levels and curtail carbonate accumulation. This variability among systems may also be due to the difference between our small alpine lake fed directly by the Sierra Nevada snowpack, and those lower elevation spring-fed meadows near smaller ranges much farther from the Pacific moisture source. The different sensitivities of geochemical and biological proxies to the immediate effects of high-frequency droughts versus the cumulative effects of long-term drought with pronounced ecological effects provides a more nuanced view of the impacts of climate on the landscape and deserves further study through a variety of proxies in multiple locations and basin types.

The Medieval Climate Anomaly (~1350–900 cal yr BP)

Two increases in carbonate accumulation in June Lake at 1220 and 890 cal yr BP (peaks 18 and 19 in Fig. 5) likely represent the dry conditions of the MCA, which appear in our records at ~1350–900 cal yr BP. First described in the region from tree ring records (Graumlich, 1993) and the age of submerged tree stumps (Stine, 1994), the MCA drought is interrupted by a pluvial interval, which is also captured in our record as a time of low carbonate accumulation and low carbonate isotope values. The drought phases of the MCA have been detected in lake records across the region (e.g., Stine, 1990; Adams et al., 2015; Zimmerman et al., 2021), though the intervening pluvial is not always well resolved (e.g., Benson et al., 2002). Owing to the combined uncertainties of our age–depth model (+/− 220 and 180 years for 1220 and 890 cal yr BP, respectively) and the radiocarbon dating of the tree stumps, the dates given here for the two droughts are offset somewhat from those first reported by Stine (1994). The MCA is known to be very dry regionally (e.g., Stine, 1990; Cook et al., 2010; Kirby et al. 2012), but as described below (see "Comparing Droughts Through Time"), %TIC and other drought indicators were less pronounced at this time than in some earlier droughts.

Recent warming and drying (~100 cal yr BP–present)

As established in Lyon et al. (2020) and Streib et al. (2021), the last ~150 years at June Lake are characterized by environmental changes likely resulting from anthropogenic warming. Diatom assemblages record an increase in lake stratification (Fig. 7), likely due to shorter winters and warmer summers (Streib et al., 2021). Further, the decline in primary productivity indicators noted in

https://doi.org/10.1017/qua.2024.38 Published online by Cambridge University Press

Lyon et al. (2020) supports a warming/drying-induced stress to the algal communities and a potential shift favoring diazotrophic cyanobacteria in June Lake over some diatoms. We note an increase in both $\delta^{18}O_{carb}$ and $\delta^{13}C_{carb}$ values over this period, which we interpret as further evidence of enhanced stratification in response to warming, despite the lack of a prominent coeval peak in Ca/Ti. However, as discussed in Lyon et al. (2020) and Streib et al. (2021), the limnology (including hydrologic closure) of the June Lake–Gull Lake system may have changed in the historical period due to anthropogenic warming, which could account for the decoupled geochemical signal. Drummond et al. (1995) noted that when lake waters warm and stratify for longer portions of the year, the dissolved inorganic carbon in the epilimnion becomes isotopically heavier, leading to higher $\delta^{13}C_{carb}$ values in authigenic carbonates. Elevated $\delta^{13}C$ values in the recent record are also consistent with increased vapor exchange with atmospheric CO_2 during dry periods (e.g., Li and Ku, 1997).

Comparing droughts through time: Differences in the MCA and LHDP

The MCA is often attributed to an increase in solar output and a decrease in low-latitude volcanic activity (e.g., Ammann et al., 2007; Mann et al., 2009), though some models also point to changes in land use (Goosse et al., 2006). In contrast, the mechanisms responsible for the LHDP are less well understood. Mensing et al. (2013) pointed to the influence of the Pacific Decadal Oscillation and its manifestation as a north–south precipitation dipole in western North America with a boundary zone at about 40–42°N (see also Wise, 2010, 2016). This would produce similar effects to the El Niño Southern Oscillation in the region, albeit at multidecadal to centennial timescales. This interpretation aligns with our observations of centennial-scale shifts from droughts to pluvials in the June Lake record throughout the LHDP.

Although several Late Holocene studies point to the MCA as a time of extreme drought (e.g., Stine, 1994; Cook et al., 2010), in some records (e.g., Stine, 1990; Mensing et al., 2013, 2023; Zimmerman et al., 2021; this study), the MCA appears to be a more modest dry interval when compared to the LHDP. At June Lake, both the TIC and Ca/Ti curves show that carbonate accumulation was lower during the MCA than during the LHDP (Fig. 5). However, the LHDP droughts are characterized by only marginally greater $\delta^{18}O_{carb}$ and $\delta^{13}C_{carb}$ values than the MCA. This poses the question: Is there a limit to ^{18}O enrichment in June Lake carbonates? A mechanism for limiting isotopic enrichment may be the seepage of ground water from June Lake to Gull Lake. This subsurface connection is suggested by the intermediate water isotope values for Gull Lake (Fig. 3). If June Lake were closed in the subsurface, we might anticipate higher $\delta^{18}O_{carb}$ during droughts. Indeed, Steinman and Abbott (2013) find that closed lake seepage acts to control longer-term hydrologically forced isotopic response: When outflow seepage is lower, lake isotopic sensitivity to hydrologic forcing declines.

Thus, although carbonate precipitation was much greater during the LHDP than the MCA, the carbonate isotope record does not exhibit a proportional response to drought conditions. Although they are positively correlated, a linear relationship between %TIC and $\delta^{18}O_{carb}$ is not obvious ($R^2 = 0.36$; P value < 0.00001 at 0.05 significance threshold). Instead, a logarithmic function would seem to better describe the relationship between these two indicators (Fig. 6C; $R^2 = 0.65$; P value < 0.00001): At %TIC values < ∼1.0%, a range of low $\delta^{18}O_{carb}$ values are possible. However, when carbonate precipitation is greater (%TIC > 1.0%), $\delta^{18}O$ values are higher and less variable, reaching a maximum of −4.4‰. We suggest that this is due to the aforementioned closed lake seepage model (Steinman and Abbott, 2013).

Although calcium limitation in some lakes may produce peaks in carbonate accumulation discordant with the expected model (e.g., Shapley et al., 2005; Zimmerman et al., 2011), June Lake has relatively high dissolved Ca^{2+} (∼24.2 mg/L in 2016; Lyon et al., 2019) and is supersaturated with respect to calcium carbonate. We also note lower pH at depth, at least during summer stratification (pH = 7.49 at 23.4 m near the coring site versus 8.7 at the surface in May 2016; Lyon et al., 2019). This may lead to some dissolution of carbonate at depth (e.g., Dean, 1999), particularly during warm/dry intervals when seasonal stratification is intense, as at present and during the MCA (Streib et al., 2021). This may explain some of the decoupling between the $\delta^{18}O$ and TIC data sets. However, additional hydrologic characterization of the system would be needed to fully test these ideas, which is beyond the scope of this study.

The LIA and other pluvials

We interpret times of low carbonate accumulation as the wettest periods, and thus as the most likely times that June Lake overflowed and connected with Gull Lake along surface flow paths (Fig. 1). One notable example is the LIA (∼500–100 cal yr BP; IPCC, 2021), a known interval of glacial re-advance and higher lake levels in the region (e.g., Stine, 1990; Kirby et al., 2010, 2012; Bowerman and Clark, 2011; Bacon et al, 2018; Thiessen et al., 2019). Further, the *Lindavia*:*Stephanodiscus* ratio for June Lake is low during the LIA, indicating a well-mixed lake (Fig. 7; Streib et al., 2021), consistent with cool conditions that would inhibit stratification and evaporative concentration of lake water. Low carbonate accumulation also occurred between ∼1800 and 1400 cal yr BP, and at ∼4300 cal yr BP in the June Lake sediment archive. Thus, although this carbonate accumulation record allows us to recognize discrete droughts over the last 4600 years, it also illuminates times of high effective moisture (Fig. 5).

Conclusions

The sedimentary record of carbonate accumulation presented here shows changes in P/E and lake level over the Late Holocene for June Lake, which lies at the eastern edge of the Sierra Nevada. When %TIC and Ca/Ti are high, so are values of $\delta^{13}C_{carb}$ and $\delta^{18}O_{carb}$, supporting the interpretation that carbonate accumulation is higher during times of drought. A lack of correlation between $\delta^{13}C_{carb}$ and $\delta^{18}O_{carb}$ indicates that June Lake is hydrologically open, likely due to groundwater seepage in the subsurface. Although surficially closed at present, June Lake may have been open at different points in the Late Holocene, including most of the LIA (∼800–300 cal yr BP), from ∼1800 to 1400 cal yr BP, and around 4300 cal yr BP, based on very low carbonate content in the sediments. Despite its closure at the surface, June Lake likely experienced subsurface outflow over most of the last 4600 years, as suggested by carbonate isotope values that do not increase linearly with carbonate precipitation. This idea has implications for paleoclimatic reconstructions that is ripe for exploration in future research.

Using the high-resolution Ca/Ti record as an archive of abrupt changes in hydroclimate over the last 4600 years, we find at least six broad intervals of centennial-scale drought, many of which can be resolved into a series of decadal to centennial-scale

https://doi.org/10.1017/qua.2024.38 Published online by Cambridge University Press

droughts (Table 4, Fig. 5). The most prominent episodes of carbonate accumulation and drought occur during the LHDP, during which there are at least seven droughts separated by several decades to ~250 years. We also find evidence of drought as early as ~3200 cal yr BP in June Lake, which is likely the earliest phase of the LHDP (Fig. 7). The LHDP has heretofore been described mainly for the eastern and central Great Basin, though it is also described in some southern California records (e.g., Kirby et al., 2014); this study adds new evidence for the timing and magnitude of the LHDP droughts in the eastern Sierra Nevada, and adds additional information to the LHDP records from the Mono Lake basin (Stine, 1990; Zimmerman et al. 2021).

Supplementary material. The supplementary material for this article can be found at https://doi.org/10.1017/qua.2024.38

Acknowledgments. A portion of this work was performed under the auspices of the U.S. Department of Energy by Lawrence Livermore National Laboratory under Contract DE-AC52-07NA27344; this is LLNL-JRNL-844307. Research at June Lake was permitted through the Inyo National Forest (USFS). Fieldwork was supported in part by the Overcash Fund for Field Research and UK alumni donors to the UK Field Geology Fund for fieldwork support. We also thank John and Mickey Frederickson at the June Lake Marina for generously allowing us to use their equipment and facilities. We are grateful to the staff of the Continental Scientific Drilling Facility for their help with core preparation, sampling, and curation. Thorough comments by several anonymous reviewers, as well as QR editors L. Anderson and N. Lancaster, improved the quality of the manuscript.

References

Adams, K.D., Negrini, R.M., Cook, E.R., Rajagopal, S., 2015. Annually resolved late Holocene paleohydrology of the southern Sierra Nevada and Tulare Lake, California. *Water Resources Research* **51**, 9708–9724.

Ammann, C.M., Joos, F., Schimel, D.S., Otto-Bliesner, B.L., Tomas, R.A., 2007. Solar influence on climate during the past millennium: results from transient simulations with the NCAR Climate System Model. *Proceedings of the National Academy of Sciences of the United States of America* **104**, 3713–3718.

Anderson, L., Berkelhammer, M., Barron, J.A., Steinman, B.A., Finney, B.P., Abbott, M.B., 2016. Lake oxygen isotopes as recorders of North American Rocky Mountain hydroclimate: Holocene patterns and variability at multi-decadal to millennial time scales. *Global and Planetary Change* **137**, 131–148.

Anderson, L., Skipp, G., Strickland, L., Honke, J., Havens, J., VanSistine, D.P., 2023. Holocene paleohydrology from alpine lake sediment, Emerald Lake, Wasatch Plateau of central Utah, USA. *Quaternary Research* **112**, 1–19.

Bacon, S.N., Lancaster, N., Stine, S., Rhodes, E.J., Holder, G.A.M., 2018. A continuous 4000-year lake-level record of Owens Lake, south-central Sierra Nevada, California, USA. *Quaternary Research* **90**, 276–302.

Benson, L., Kashgarian, M., Rye, R., Lund, S., Paillet, F., Smoot, J., Kester, C., Mensing, S., Meko, D., Lindström, S., 2002. Holocene multidecadal and multicentennial droughts affecting Northern California and Nevada. *Quaternary Science Reviews* **21**, 659–682.

Blaauw, M., Christen, J.A., 2011. Flexible paleoclimate age-depth models using an autoregressive gamma process. *Bayesian Analysis* **6**, 457–474.

Bowen, G.J., 2011. The Online Isotopes in Precipitation Calculator (accessed August 18, 2021). https://wateriso.utah.edu/waterisotopes/pages/data_access/oipc.html

Bowen, G.J., Revenaugh, J., 2003. Interpolating the isotopic composition of modern meteoric precipitation. *Water Resources Research* **39**. https://doi.org/10.1029/2003WR002086

Bowerman, N.D., Clark, D.H., 2011. Holocene glaciation of the central Sierra Nevada, California. *Quaternary Science Reviews* **30**, 1067–1085.

Braconnot, P., Harrison, S.P., Kageyama, M., Bartlein, P.J., Masson-Delmotte, V., Abe-Ouchi, A., Otto-Bliesner, B., Zhao, Y., 2012. Evaluation of climate models using palaeoclimatic data. *Nature Climate Change* **2**, 417–424.

Brooks, J.R., Gibson, J.J., Birks, S.J., Weber, M.H., Rodecap, K.D., Stoddard, J.L., 2014. Stable isotope estimates of evaporation: inflow and water residence time for lakes across the United States as a tool for national lake water quality assessments. *Limnology and Oceanography* **59**, 2150–2165.

Bursik, M., Sieh, K., 2013. Digital database of the Holocene tephras of the Mono-Inyo Craters, California. U.S. Geological Survey Data Series 758 (accessed 15 February 2022). https://pubs.usgs.gov/ds/758/

Cayan, D.R., Peterson, D.H.,1989. The influence of North Pacific atmospheric circulation on streamflow in the west. In: Peterson, D.H. (Ed.), *Aspects of Climate Variability in the Pacific and the Western Americas*. Geophysical Monograph Series 55. American Geophysical Union, Washington, DC, pp. 375–397.

Cook, E.R., Seager, R., Heim, R.R. Jr., Vose, R.S., Herweijer, C., Woodhouse, C., 2010. Megadroughts in North America: placing IPCC projections of hydroclimatic change in a long-term palaeoclimate context. *Journal of Quaternary Science* **25**, 48–61.

Coplen, T.B., Brand, W.A., Gehre, M., Gröning, M., Meijer, H.A.J., Toman, B., Verkouteren, R.M., 2006. New guidelines for $\delta^{13}C$ measurements. *Analytical Chemistry* **78**, 2439–2441.

Daëron, M., Drysdale, R.N., Peral, M., Huyghe, D., Blamart, D., Coplen, T.B., Lartaud, F., Zanchetta, G., 2019. Most Earth-surface calcites precipitate out of isotopic equilibrium. *Nature Communications* **10**, 429. https://doi.org/10.1038/s41467-019-08336-5

Dansgaard, W., 1964. Stable isotopes in precipitation. *Tellus A: Dynamic Meteorology and Oceanography* **16**, 436–468.

Davies, S.J., Lamb, H.F., Roberts, S.J., 2015. Micro-XRF core scanning in palaeolimnology: recent developments. In: Croudace, I.W., Rothwell, R.G. (Eds.), *Micro-XRF Studies of Sediment Cores*. Springer Netherlands, Dordrecht, pp. 189–226.

Dean, W.E., 1999. The carbon cycle and biogeochemical dynamics in lake sediments. *Journal of Paleolimnology* **21**, 375–393.

Dettinger, M., 2011. Climate change, atmospheric rivers, and floods in California – a multimodel analysis of storm frequency and magnitude changes. *Journal of the American Water Resources Association* **47**, 514–523.

Dettinger, M.D., 2013. Atmospheric rivers as drought busters on the U.S. West Coast. *Journal of Hydrometeorology* **14**, 1721–1732.

Diffenbaugh, N.S., Swain, D.L., Touma, D., 2015. Anthropogenic warming has increased drought risk in California. *Proceedings of the National Academy of Sciences of the United States of America* **112**, 3931–3936.

Drummond, C.N., Patterson, W.P., Walker, J.C.G., 1995. Climatic forcing of carbon-oxygen isotopic covariance in temperate-region marl lakes. *Geology* **23**, 1031–1034.

Friedman, I., Redfield, A.C., Schoen, B., Harris, J., 1964. The variation of the deuterium content of natural waters in the hydrologic cycle. *Reviews of Geophysics* **2**, 177–224.

Friedman, I., Smith, G.I., Gleason, J.D., Warden, A., Harris, J.M., 1992. Stable isotope composition of waters in southeastern California 1. Modern precipitation. *Journal of Geophysical Research: Atmospheres* **97**, 5795–5812.

Goosse, H., Arzel, O., Luterbacher, J., Mann, M.E., Renssen, H., Riedwyl, N., Timmermann, A., Xoplaki, E., Wanner, H., 2006. The origin of the European "Medieval Warm Period." *Climate of the Past* **2**, 99–113.

Goss, M., Swain, D., Abatzoglou, J., Sarhadi, A., Kolden, C.A., Williams, A.P., Diffenbaugh, N.S., 2020. Climate change is increasing the likelihood of extreme autumn wildfire conditions across California. *Environmental Research Letters* **15**, 094016. https://doi.org/10.1088/1748-9326/ab83a7

Graumlich, L.J., 1993. A 1000-year record of temperature and precipitation in the Sierra Nevada. *Quaternary Research* **39**, 249–255.

Greenblat, A.T., Allen, D.M., Hahm, W.J., 2024. Characterizing isotopic composition and trajectories of atmospheric river events. *Atmosphere* **15**, 74. https://doi.org/10.3390/atmos15010074

Guan, B., Molotch, N.P., Waliser, D.E., Fetzer, E.J., Neiman, P.J., 2010. Extreme snowfall events linked to atmospheric rivers and surface air

temperature via satellite measurements. *Geophysical Research Letters* **37**, 2010GL044696. https://doi.org/10.1029/2010GL044696

Guan, B., Molotch, N.P., Waliser, D.E., Fetzer, E.J., Neiman, P.J., 2013. The 2010/2011 snow season in California's Sierra Nevada: role of atmospheric rivers and modes of large-scale variability. *Water Resources Research* **49**, 6731–6743.

Hammer, Ø., Harper, D., Ryan, P., 2001. PAST: Paleontological statistics software package for education and data analysis. *Palaeontologia Electronica* **4**, 1–9.

Holmes, J.A., De Deckker, P., 2012. The chemical composition of ostracod shells. *Developments in Quaternary Sciences* **17**, 131–143.

Horton, T.W., Defliese, W.F., Tripati, A.K., Oze, C., 2015. Evaporation induced ^{18}O and ^{13}C enrichment in lake systems: a global perspective on hydrologic balance effects. *Quaternary Science Reviews: Water Isotope Systematics* **131**, 365–379.

Huang, X., Hall, A.D., Berg, N., 2018. Anthropogenic warming impacts on today's Sierra Nevada snowpack and flood risk. *Geophysical Research Letters* **45**, 6215–6222.

IPCC, 2021. *Climate Change 2021: The Physical Science Basis: Working Group I Contribution to the Sixth Assessment Report of the Intergovernmental Panel on Climate Change*. 1st ed. Cambridge University Press, Cambridge.

Jasechko, S., Sharp, Z.D., Gibson, J.J., Birks, S.J., Yi, Y., Fawcett, P.J., 2013. Terrestrial water fluxes dominated by transpiration. *Nature* **496**, 347–350.

John, D., duBray, E., Blakely, R., Fleck, R., Vikre, P., Box, S., Moring, B., 2012. Miocene magmatism in the Bodie Hills volcanic field, California and Nevada: a long-lived eruptive center in the southern segment of the ancestral Cascades arc. *Geosphere* **8**, 44. https://doi.org/10.1130/GES00674.1

Kaufman, D., McKay, N., Routson, C., Erb, M., Davis, B., Heiri, O., Jaccard, S., *et al.*, 2020. A global database of Holocene paleotemperature records. *Scientific Data* **7**, 115. https://doi.org/10.1038/s41597-020-0445-3

Kelts, K., Hsü, K.J., 1978. Freshwater carbonate sedimentation. In: Lerman, A. (Ed.), *Lakes: Chemistry, Geology, Physics*. Springer, New York, pp. 295–323.

Kirby, M.E.C., Patterson, W.P., Lachniet, M., Noblet, J.A., Anderson, M.A., Nichols, K., Avila, J., 2019. Pacific Southwest United States Holocene droughts and pluvials inferred from sediment $\delta^{18}O$(calcite) and grain size data (Lake Elsinore, California). *Frontiers in Earth Science* **7**, 74. https://doi.org/10.3389/feart.2019.00074

Kirby, M.E., Feakins, S.J., Hiner, C.A., Fantozzi, J., Zimmerman, S.R.H., Dingemans, T., Mensing, S.A., 2014. Tropical Pacific forcing of Late-Holocene hydrologic variability in the coastal southwest United States. *Quaternary Science Reviews* **102**, 27–38.

Kirby, M.E., Lund, S.P., Patterson, W.P., Anderson, M.A., Bird, B.W., Ivanovici, L., Monarrez, P., Nielsen, S., 2010. A Holocene record of Pacific Decadal Oscillation (PDO)-related hydrologic variability in Southern California (Lake Elsinore, CA). *Journal of Paleolimnology* **44**, 819–839.

Kirby, M.E., Zimmerman, S.R.H., Patterson, W.P., Rivera, J.J., 2012. A 9170-year record of decadal-to-multi-centennial scale pluvial episodes from the coastal Southwest United States: a role for atmospheric rivers? *Quaternary Science Reviews* **46**, 57–65.

Kylander, M., Ampel, L., Wohlfarth, B., Veres, D., 2011. High-resolution X-ray fluorescence core scanning analysis of Les Echets (France) sedimentary sequence: new insights from chemical proxies. *Journal of Quaternary Science* **26**, 109–117.

Lafuente, B., Downs, R.T., Yang, H., Stone, N., 2016. 1. The power of databases: the RRUFF project. In: Armbruster, T., Danisi, R.M. (Eds.), *Highlights in Mineralogical Crystallography*. De Gruyter, Berlin, pp. 1–30.

Leng, M.J., Marshall, J.D., 2004. Palaeoclimate interpretation of stable isotope data from lake sediment archives. *Quaternary Science Reviews* **23**, 811–831.

Li, H.-C., Ku, T.-L., 1997. $\delta^{13}C$–$\delta^{18}C$ covariance as a paleohydrological indicator for closed-basin lakes. *Palaeogeography, Palaeoclimatology, Palaeoecology* **133**, 69–80.

Li, H.-C., Ku, T.-L., Stott, L.D., Anderson, R.F., 1997. Stable isotope studies on Mono Lake (California). 1. d18 in lake sediments as proxy for climatic change during the last 150 years. *Limnology and Oceanography* **42**, 230–238.

Liu, X., Colman, S.M., Brown, E.T., Minor, E.C., Li, H., 2013. Estimation of carbonate, total organic carbon, and biogenic silica content by FTIR and XRF techniques in lacustrine sediments. *Journal of Paleolimnology* **50**, 387–398.

Lopera-Congote, L., Westover, K., McGlue, M.M., Yeager, K.M., Streib, L.C., Stone, J.R., 2024. Detecting climate-driven ecological changes in high-altitude lakes in the Sierra Nevada, California. *The Holocene* **34**, 870–880.

Lyon, E.C., McGlue, M.M., Erhardt, A.M., Kim, S.L., Stone, J.R., Zimmerman, S.R.H., 2020. Late Holocene hydroclimate changes in the eastern Sierra Nevada revealed by a 4600-year paleoproduction record from June Lake, CA. *Quaternary Science Reviews* **242**, 106432. https://doi.org/10.1016/j.quascirev.2020.106432

Lyon, E.C., McGlue, M.M., Woolery, E.W., Kim, S.L., Stone, J.R., Zimmerman, S.R.H., 2019. Sublacustrine geomorphology and modern sedimentation in a glacial scour basin, June Lake, eastern Sierra Nevada, U.S.A. *Journal of Sedimentary Research* **89**, 919–934.

Mann, M.E., Zhang, Z., Rutherford, S., Bradley, R.S., Hughes, M.K., Shindell, D., Ammann, C., Faluvegi, G., Ni, F., 2009. Global signatures and dynamical origins of the Little Ice Age and Medieval Climate Anomaly. *Science* **326**, 1256–1260.

McCormack, J., Kwiecien, O., 2021. Coeval primary and diagenetic carbonates in lacustrine sediments challenge palaeoclimate interpretations. *Scientific Reports* **11**, 7935. https://doi.org/10.1038/s41598-021-86872-1

Mensing, S.A., Benson, L.V., Kashgarian, M., Lund, S., 2004. A Holocene pollen record of persistent droughts from Pyramid Lake, Nevada, USA. *Quaternary Research* **62**, 29–38.

Mensing, S.A., Sharpe, S.E., Tunno, I., Sada, D.W., Thomas, J.M., Starratt, S., Smith, J., 2013. The Late Holocene Dry Period: multiproxy evidence for an extended drought between 2800 and 1850 cal yr BP across the central Great Basin, USA. *Quaternary Science Reviews* **78**, 266–282.

Mensing, S., Wang, W., Rhode, D., Kennett, D.J., Csank, A., Thomas, D.H., Briem, C., *et al.*, 2023. Temporal and geographic extent of the late Holocene dry period in the central Great Basin, USA. *Quaternary Science Reviews* **300**, 107900. https://doi.org/10.1016/j.quascirev.2022.107900

Millar, C.I., Charlet, D.A., Delany, D.L., King, J.C., Westfall, R.D., 2019. Shifts of demography and growth in limber pine forests of the Great Basin, USA, across 4000 yr of climate variability. *Quaternary Research* **91**, 691–704.

Myrbo, A., 2013. Making Smear Slides. Tool for Microscopic Identification, University of Minnesota https://tmi.csd.umn.edu/module/blogpost?postURL=https%3A%2F%2Fwww.googleapis.com%2Fblogger%2Fv2%2Fblogs%2F8153395487262690384%2Fposts%2F7700420303326032910 (accessed January 4, 2024).

Oremland, R.S., Miller, L.G., Whiticar, M.J., 1987. Sources and flux of natural gases from Mono Lake, California. *Geochimica et Cosmochimica Acta* **51**, 2915–2929.

Peltier, J.M., 2023. Establishing a Stable Isotope Profile for Atmospheric River Events in Northern California. Master's thesis, California State University, Sacramento.

Pyke, C.B., 1972. Some Meteorological Aspects of the Seasonal Distribution of Precipitation in the Western United States and Baja California. PhD dissertation, University of California Los Angeles.

Ralph, F.M., Dettinger, M.D., 2011. Storms, floods, and the science of atmospheric rivers. *Eos, Transactions American Geophysical Union* **92**, 265–266.

Rhoades, A.M., Jones, A.D., Srivastava, A., Huang, H., O'Brien, T.A., Patricola, C.M., Ullrich, P.A., Wehner, M., Zhou, Y., 2020. The shifting scales of Western U.S. landfalling atmospheric rivers under climate change. *Geophysical Research Letters* **47**, e2020GL089096. https://doi.org/10.1029/2020GL089096

Schnurrenberger, D., Russell, J., Kelts, K., 2003. Classification of lacustrine sediments based on sedimentary components. *Journal of Paleolimnology* **29**, 141–154. https://doi.org/10.1023/A:1023270324800

Shapley, M.D., Ito, E., Donovan, J.J., 2005. Authigenic calcium carbonate flux in groundwater-controlled lakes: implications for lacustrine paleoclimate records. *Geochimica et Cosmochimica Acta* **69**, 2517–2533.

Steinman, B.A., Abbott, M.B., 2013. Isotopic and hydrologic responses of small, closed lakes to climate variability: hydroclimate reconstructions from lake sediment oxygen isotope records and mass balance models. *Geochimica et Cosmochimica Acta* **105**, 342–359.

https://doi.org/10.1017/qua.2024.38 Published online by Cambridge University Press

Stine, S., 1990. Late Holocene fluctuations of Mono Lake, eastern California. *Palaeogeography, Palaeoclimatology, Palaeoecology* **78**, 333–381.

Stine, S., 1994. Extreme and persistent drought in California and Patagonia during mediaeval time. *Nature* **369**, 546–549.

Streib, L.C., Stone, J.R., Lyon, E.C., Quang, H.H., Yeager, K.M., Zimmerman, S.R.H., McGlue, M.M., 2021. Anthropogenic climate change has altered lake state in the Sierra Nevada (California, USA). *Global Change Biology* **27**, 6059–6070.

Sun, F., Berg, N., Hall, A., Schwartz, M., Walton, D., 2019. Understanding end-of-century snowpack changes over California's Sierra Nevada. *Geophysical Research Letters* **46**, 933–943.

Talbot, M.R., 1990. A review of the palaeohydrological interpretation of carbon and oxygen isotopic ratios in primary lacustrine carbonates. *Chemical Geology: Isotope Geoscience section* **80**, 261–279.

Talbot, M.R., Kelts, K., 1990. Paleolimnological signatures from carbon and oxygen isotopic ratios in carbonates, from organic carbon-rich lacustrine sediments. In: Katz, B.J. (Ed.), *Lacustrine Basin Exploration: Case Studies and Modern Analogs*. AAPG Memoir 50. American Association of Petroleum Geologists, Tulsa, OK, pp. 99–112.

Theissen, K.M., Hickson, T.A., Brundrett, A.L., Horns, S.E., Lachniet, M.S., 2019. A record of mid- and late Holocene paleohydroclimate from Lower Pahranagat Lake, southern Great Basin. *Quaternary Research* **92**, 352–364.

Tomascak, P.B., Hemming, N.G., Hemming, S.R., 2003. The lithium isotopic composition of waters of the Mono Basin, California. *Geochimica et Cosmochimica Acta* **67**, 601–611.

Ullrich, P.A., Xu, Z., Rhoades, A.M., Dettinger, M.D., Mount, J.F., Jones, A.D., Vahmani, P., 2018. California's drought of the future: a midcentury recreation of the exceptional conditions of 2012–2017. *Earth's Future* **6**, 1568–1587.

Williams, A.P., Cook, B.I., Smerdon, J.E., 2022. Rapid intensification of the emerging southwestern North American megadrought in 2020–2021. *Nature Climate Change* **12**, 232–234.

Wise, E.K., 2010. Spatiotemporal variability of the precipitation dipole transition zone in the western United States. *Geophysical Research Letters* **37**, 2009GL042193. https://doi.org/10.1029/2009GL042193

Wise, E.K., 2016. Five centuries of U.S. West Coast drought: occurrence, spatial distribution, and associated atmospheric circulation patterns. *Geophysical Research Letters* **43**, 4539–4546.

Zimmerman, S.R.H., Hemming, S.R., Hemming, N.G., Tomascak, P.B., Pearl, C., 2011. High-resolution chemostratigraphic record of late Pleistocene lake-level variability, Mono Lake, California. *Geological Society of America Bulletin* **123**, 2320–2334.

Zimmerman, S.R.H., Hemming, S.R., Starratt, S.W., 2021. Holocene sedimentary architecture and paleoclimate variability at Mono Lake, California. In: Starratt, S.W., Rosen, M.R. (Eds.), *From Saline to Freshwater: The Diversity of Western Lakes in Space and Time*. GSA Special Papers 536. Geological Society of America, Boulder, CO, pp. 399–434.

Zimmerman, S.R.H., Wahl, D.B., 2020. Holocene paleoclimate change in the western US: the importance of chronology in discerning patterns and drivers. *Quaternary Science Reviews* **246**, 106487. https://doi.org/10.1016/j.quascirev.2020.106487

https://doi.org/10.1017/qua.2024.38 Published online by Cambridge University Press